








Article

Urokinase-Type Plasminogen Activator Receptor (uPAR) Cooperates with Mutated *KRAS* in Regulating Cellular Plasticity and Gemcitabine Response in Pancreatic Adenocarcinomas

Luogen Peng ^{1,2}, Yuchan Li ¹, Sha Yao ^{1,3}, Jochen Gaedcke ⁴, Victor M. Baart ⁵, Cornelis F. M. Sier ⁵, Albrecht Neesse ^{6,7}, Volker Ellenrieder ⁶, Hanibal Bohnenberger ¹, Frieder Fuchs ^{1,8,9}, Julia Kitz ¹, Philipp Ströbel ^{1,*} and Stefan Küffer ¹

- ¹ Institute of Pathology, University Medical Center Göttingen, University of Göttingen, 37075 Göttingen, Germany
 - ² Department of Oncology, Changsha Central Hospital, University of South China, Changsha 410004, China
 - ³ Department of Pathology, The 3rd Xiangya Hospital, Central South University, Changsha 410013, China
 - ⁴ Department of General, Visceral and Pediatric Surgery, University Medical Center Göttingen, 37075 Göttingen, Germany
 - ⁵ Department of Surgery, Leiden University Medical Center, 2333 ZA Leiden, The Netherlands
 - ⁶ Department of Gastroenterology and Gastrointestinal Oncology, University Medical Center Göttingen, 37075 Göttingen, Germany
 - ⁷ Department of Medicine, Israelitisches Krankenhaus, 22297 Hamburg, Germany
 - ⁸ Department of Microbiology and Hospital Hygiene, Bundeswehr Central Hospital Koblenz, 56070 Koblenz, Germany
 - ⁹ Institute for Medical Microbiology, Immunology and Hygiene, University of Cologne, Medical Faculty and University Hospital of Cologne, 50931 Cologne, Germany
- * Correspondence: philipp.stroebel@med.uni-goettingen.de; Tel.: +49-551-39-65681



Citation: Peng, L.; Li, Y.; Yao, S.; Gaedcke, J.; Baart, V.M.; Sier, C.F.M.; Neesse, A.; Ellenrieder, V.; Bohnenberger, H.; Fuchs, F.; et al. Urokinase-Type Plasminogen Activator Receptor (uPAR) Cooperates with Mutated *KRAS* in Regulating Cellular Plasticity and Gemcitabine Response in Pancreatic Adenocarcinomas. *Cancers* **2023**, *15*, 1587. <https://doi.org/10.3390/cancers15051587>

Academic Editor: Louis Buscail

Received: 30 January 2023
Revised: 27 February 2023
Accepted: 28 February 2023
Published: 3 March 2023



Copyright: © 2023 by the authors. Licensee MDPI, Basel, Switzerland. This article is an open access article distributed under the terms and conditions of the Creative Commons Attribution (CC BY) license (<https://creativecommons.org/licenses/by/4.0/>).

Simple Summary: Pancreatic ductal adenocarcinomas (PDACs) with gene amplification or over-expression of urokinase-type plasminogen activator receptor (uPAR) have a particularly dismal prognosis. We show here that uPAR reinforces the MEK/ERK signaling pathway in tumor cells with a *KRAS* mutation with the suppression of FAK and CDC42 signaling. This synergy keeps tumor cells in a mesenchymal state that favors cell migration and proliferation, but also sensitizes them towards gemcitabine. These observations highlight a potential therapeutic dilemma that applies to *KRAS* and uPAR as emerging targets. Treatments targeting either *KRAS* or uPAR could induce cellular dormancy and render the tumor more resistant to chemotherapy (such as gemcitabine). The clinical benefit of adding autophagy inhibitors such as chloroquine in this situation remains to be shown.

Abstract: Background: Pancreatic ductal adenocarcinoma (PDAC) remains one of the most lethal cancers. Given the currently limited therapeutic options, the definition of molecular subgroups with the development of tailored therapies remains the most promising strategy. Patients with high-level gene amplification of urokinase plasminogen activator receptor (*uPAR/PLAUR*) have an inferior prognosis. We analyzed the uPAR function in PDAC to understand this understudied PDAC subgroup's biology better. Methods: A total of 67 PDAC samples with clinical follow-up and TCGA gene expression data from 316 patients were used for prognostic correlations. Gene silencing by CRISPR/Cas9, as well as transfection of *uPAR* and mutated *KRAS*, were used in PDAC cell lines (AsPC-1, PANC-1, BxPC3) treated with gemcitabine to study the impact of these two molecules on cellular function and chemoresponse. HNF1A and KRT81 were surrogate markers for the exocrine-like and quasi-mesenchymal subgroup of PDAC, respectively. Results: High levels of uPAR were correlated with significantly shorter survival in PDAC, especially in the subgroup of HNF1A-positive exocrine-like tumors. uPAR knockout by CRISPR/Cas9 resulted in activation of FAK, CDC42, and p38, upregulation of epithelial makers, decreased cell growth and motility, and resistance against gemcitabine that could be reversed by re-expression of uPAR. Silencing of *KRAS* in AsPC1 using siRNAs reduced uPAR levels significantly, and transfection of mutated *KRAS* in BxPC-3 cells rendered

the cell more mesenchymal and increased sensitivity towards gemcitabine. Conclusions: Activation of uPAR is a potent negative prognostic factor in PDAC. uPAR and KRAS cooperate in switching the tumor from a dormant epithelial to an active mesenchymal state, which likely explains the poor prognosis of PDAC with high uPAR. At the same time, the active mesenchymal state is more vulnerable to gemcitabine. Strategies targeting either KRAS or uPAR should consider this potential tumor-escape mechanism.

Keywords: pancreatic cancer; uPAR; KRAS; FAK; MEK; ERK; dormancy; gemcitabine

1. Introduction

Pancreatic ductal adenocarcinomas (PDACs) are among the human tumors with the worst prognosis. Most PDAC patients are already at an advanced stage at diagnosis, and resection as the most effective treatment is only feasible in 20% of patients [1]. With gemcitabine as a baseline combined with FOLFIRINOX, next to albumin-bound paclitaxel, therapeutic options are limited [2–4]. The current clinical staging of PDAC cannot fully predict tumor behavior, and the prognosis of patients receiving the same treatment varies considerably. Therefore, it is essential to develop robust molecular classifications of PDAC for more tailored therapeutic approaches [5]. An increasing number of molecular and histological subtypes already define subtype-specific therapeutic vulnerabilities and provide the opportunity to supplement current pathological classifications. Recent studies discovered many PDAC subtype-specific markers connected to different clinical behavior; however, the three main subtypes remain classical, quasi-mesenchymal (QM-PDA), and exocrine-like [6].

Nevertheless, there is now good evidence that cancer cells preserve cellular plasticity [7,8]. Increased levels of urokinase-type plasminogen activator receptor (uPAR) are associated with early invasion, metastasis, and poor prognosis in many solid and hematological tumors, including PDAC [9–11]. uPAR is a GPI-anchored cell membrane receptor without an intracellular domain that mediates the degradation of extracellular matrix (ECM) components [12], including fibronectin and vitronectin [13]. It locally increases plasmin activity that facilitates cell migration. Interaction of uPAR with integrins occurs indirectly through stabilized binding to vitronectin [14]. This leads to intracellular activation of the Ras pathway, the focal adhesion kinase (FAK), and the Rho family small GTPase Rac (reviewed in [15]). PDAC is also one of the tumors with the highest frequency of KRAS mutations. KRAS has not only been shown to activate cell proliferation through RAF/MEK/ERK [16]; it has also been reported to regulate uPAR expression by AP1-dependent transactivation of the *uPAR* promoter [17]. Downregulation or blocking of uPAR causes activation of FAK, Src, CDC42, and p38, resulting in cell-cycle arrest and dormancy [18,19].

We have previously shown that 50% of PDACs show overexpression of uPAR due to low or high-level amplifications of the uPAR gene *PLAUR*. These tumors are associated with an inferior prognosis [20]. In this study, we functionally studied the role of uPAR in cell lines and validated the results in a cohort of 67 PDAC patients with clinical follow-up supplemented by TCGA data of 316 PDAC patient samples.

2. Materials and Methods

2.1. Human Tissue Samples

Tumor samples from 67 PDAC patients organized on a multi-tissue array (TMA) were used for immunohistochemical staining (clinical data are summarized in Table 1). The patient sample collection was approved by the ethics committee of the University Medical Center Göttingen (GÖ 912/15).

Table 1. Clinical data summary.

Patients	67
Male (%)	37 (55)
Female (%)	30 (45)
Age median (range)	68 (44–84)
Tumor grade (G)	
1–2 (%)	6 (9)
2–3 (%)	41 (61.1)
3–4 (%)	20 (29.9)
Tumor stage (TNM)	
T 1 (%)	1 (1.5)
T 2 (%)	3 (4.5)
T 3 (%)	58 (86.6)
T 4 (%)	5 (7.4)
N 0 (%)	14 (20.9)
N 1–3 (%)	53 (79.1)
Median follow-up time (range) [day]	417 (4–2768)
Reported deaths (%)	62 (92.5)

2.2. Immunohistochemistry

Immunohistochemical staining (IHC) of 2 μ m paraffin sections was performed according to standard methods. Briefly, after deparaffinization in serially diluted alcohol and blocking endogenous peroxidase in 0.3% hydrogen peroxide in PBS, antigen retrieval was performed at 95 °C in either a low or high-pH Envision FLEX target retrieval solution (Agilent, Santa Clara, CA, USA) using PT Link (Agilent). Subsequently, the stainings were incubated for 1 h with primary antibodies, followed by washing in PBS and incubation with the appropriate detection system for 30 min (Envision, Agilent). Antibodies were used at predetermined optimal dilutions (Supplementary Table S3) with the proper positive and negative controls. Staining was visualized by 3,3'-diaminobenzidine tetrahydrochloride solution, counterstained with hematoxylin, dehydrated, and mounted in Pertex. Using an H-score, all tissue samples were evaluated for nuclear staining of p-p38, uPA, uPAR, and PAI1. The H-score was calculated by $3 \times$ the percentage of the strongest staining signal + $2 \times$ the percentage of a moderate signal + the percentage of a weak signal, resulting in a value range from 0 to 300. HNF1A and KRT81 were graded for “low” or “high” expression according to signal intensity. The optimal levels for the discrimination between high and low signals of uPAR, HNF1A, and KRT81 were determined using the cutoff finder [21].

2.3. Cell Culture and Transient Expression of uPAR and KRAS^{G12C}

The human pancreatic cancer cell lines BxPC-3, AsPC-1, CAPAN-2, MIA PaCa-2, PATU8988T, and PANC-1 were obtained from the American Type Culture Collection (ATCC) (Supplementary Table S1). All cells were grown in RPMI-1640 medium (Gibco, Waltham, MA, USA), supplemented with 10% FCS (Gibco), 1% L-glutamine (Gibco), and 1% Penicillin/Streptomycin (Gibco) under humidified conditions at 37 °C and 5% CO₂. PANC-1 was transfected with the pCMV-AC-GFP vector PLAUR (NM_002659) human-tagged ORF clone (Origene, Rockville, MD, USA), and BxPC-3 with the pCMV6-Entry-KRAS^{G12C} vector (Origene Technologies Inc., Rockville, MD, USA) using the X-tremeGENE HP DNA transfection reagent (Merck, Darmstadt, Germany). Transfected cells were selected with G418 (400 ng/ μ L). uPAR protein levels were tested by ELISA as described above. KRAS^{G12C}-expressing cells were selected using 2 μ g/mL puromycin.

2.4. Generation of ASPC-1 uPAR Knockouts by CRISPR/Cas9

The uPAR CRISPR/Cas9 knockout strategy is shown in Supplementary Figure S1. Cells were transfected with two CRISPR/Cas9 constructs, pCMV-Cas9-RFP (target site: 5'-GGACCCTGAGCTATCGGACTGG-3'), and pCMV-Cas9-GFP (target site: 5'-

AGGTAACGGCTTCGGGAATAGG-3') (Sigma-Aldrich, Darmstadt, Germany) using the X-tremeGENE HP DNA transfection reagent (Merck, Rahway, NJ, USA) according to the manufacturer's instructions. After transient CRISPR/Cas9 activation, fluorescence-activated cell sorting (FACS) of GFP/RFP double-positive cells was performed for clone selection. PCR-screened clones for the gRNA target site or a potential deletion, as described later (Supplementary Figure S1). Clones that were heterozygous for the deletion were further screened for specific gRNA target site mutations by Sanger sequencing (Supplementary Figure S2)

2.5. Genomic PCR and Sanger Sequencing

The gRNA target sites were amplified with the primers GFP F: 5'-CTGTCCCCATGGAGTCTCAC-3', GFP R: 5'-CATCCAGGCACTGTTCTTCA-3', RFP F: 5'-CTGGAGCTGGTGGAGAAAAG-3', and RFP R: 5'-GGATTGGGATGATGATGAGG-3' using MyTaq™ Mix (BioLine, London, UK) and the PCR products were analyzed via QIAxcel (Qiagen, Hilden, Germany). The PCR product was purified with ExoSAP-IT™ (Applied Biosystems, Foster City, CA, USA), and sequenced according to Sanger sequencing using the BigDye® terminator v3.1 cycle sequencing kit (Applied Biosystems, Waltham, MA, USA). Sequences were analyzed using an ABI 3500 genetic analyzer (Applied Biosystems).

2.6. Cell Viability Assay

The CellTiter 96® Aqueous one-solution cell-proliferation assay (MTS, Promega, Madison, WI, USA) was performed according to the manufacturer's recommendations. In brief, 1×10^4 cells were grown in a 96-well format in 100 µL/medium and treated with indicated conditions over different periods, as described under results. Then, 20 µL of the MTS reagent was added and incubated for 1–3 h at 37 °C, and the absorbance was measured at 490 nm and 655 nm. Relative cell viability after treatment was calculated by normalizing each value by the mean of the untreated control replicates. Unless stated otherwise, all experiments were conducted by pretreating cells with 80 nM of the specific siRNA or inhibitors for 24 h and subsequent treatment with 0.1 µM gemcitabine for 72 h.

2.7. Wound Healing Assay

siRNA or mock-transfected cells were grown to almost 100% confluency before synchronizing the cells by decreasing FCS to 1% for 24 h. Wounds were created by scratching the cell monolayer with a 100 µL sterile pipette tip. Wound healing was monitored at 0, 24, and 48 h. Relative wound healing was calculated by measuring the mean distance at three defined positions of the scratch expressed as a percentage of the 0 h control.

2.8. siRNA Knockdown Experiments

siRNA transfection was performed using HiPerFect transfection reagent (Qiagen) as described elsewhere [22]. In brief, 80 nM of gene-specific or negative control siRNA (all Star Negative Control, Qiagen) was incubated with 12 µL HiPerFect in 100 µL transfection medium containing serum-free RPMI at RT for 20 min and added to freshly seeded cells (3×10^5 cells). After 24 h or 48 h incubation, cells were further processed as indicated. siRNAs used were purchased from Qiagen and are summarized in Supplementary Table S2.

2.9. Protein Extracts, Western Blot Analyses, and uPAR Quantification by ELISA

Cells at 60–70% confluency were treated as indicated in the results section. Cells were washed in PBS and scraped in a 100 µL RIPA lysis buffer containing protease inhibitor cOmplete (Roche, Mannheim, Germany), PMSF (1 mM), and orthovanadate (1 mM). Total protein was quantified using a DC™ protein assay (Bio-Rad, Hercules, CA, USA). A total of 15 µg of proteins was separated using gradient SDS gels (4–20%, Bio-Rad) and blotted on nitrocellulose membranes by a Turbo Blot (Bio-Rad). Gene signals were detected as described before [23].

uPAR protein levels were determined by ELISA (DUP00, R&D Systems, Minneapolis, USA) according to the manufacturer's protocol. In brief, cell lysates from 10^5 to 10^6 cells were 10-fold diluted in a RIPA lysis buffer, and 50 μ L of cell lysates or standard was added to 100 μ L of assay diluent RD1W solution. The samples were incubated for two hours at RT and washed four times with a 400 μ L wash buffer. A total of 200 μ L of human uPAR conjugate was added and incubated for 2 h at RT. After four washing steps, 200 μ L of substrate solution was added and incubated for 30 min at RT protected from light before adding 50 μ L of stop solution. The optical density was measured at 450 nm with a reference of 540 nm on a Tecan reader Infinite 200 Pro. uPAR concentrations were calculated for 10^6 cells.

2.10. KRAS Activity Measurement

KRAS activity was quantified using the STA-400-K-T assay (Cell Biolabs) following the manufacturer's instructions. In brief, 1 mg protein was subjected to raf1 RBD agarose beads and incubated at 4 °C for one h. Beads were pelleted, washed, and resuspended in 4 \times Laemmle buffer. KRAS activity was quantified by Western blotting of 20 μ g supernatant protein.

2.11. Statistical Analysis

Statistical analysis and AUC estimation were performed using GraphPad 8.3.0. Data are shown as mean \pm SEM. Two group comparisons were performed using Student's *t*-test. Two-way ANOVA was applied to compare cell growth and resistance analyses. Survival was analyzed using the Kaplan–Meier test and significance was evaluated using the log-rank (Cox–Mantel) test. A *p*-value of < 0.05 was considered significant (* = *p* < 0.05, ** = *p* < 0.01, *** = *p* < 0.001).

3. Results

3.1. uPAR Protein and mRNA Expression Levels Have Prognostic Significance in PDAC

Our previous study showed that *uPAR* gene amplification in PDAC correlates with poor prognosis [24]. Immunohistochemical (IHC) staining for uPAR, its ligand uPA, and the inhibitor PAI1 in a clinical cohort of 67 patients (Figure 1, Table 1) also confirmed a prognostic relevance of uPAR on the protein level. Patients with high uPAR expression (*n* = 46) had significantly shorter overall survival (OS) than patients with low uPAR levels (*n* = 23) (median survival 320 days in uPAR^{high} vs. 603 days in uPAR^{low} patients, log-rank (Cox–Mantel) test, *p* = 0.0273) (Figure 1b) [25]. Using gene expression data from two TCGA datasets including 312 PDAC patients [26,27], patients with high uPAR mRNA expression had a significantly reduced OS compared to patients with tumors of low expression (log-rank (Cox–Mantel) test, *p* = 0.0099) (Figure 1c). IHC did not reveal any significant difference in OS for uPA and PAI1 (Supplementary Figure S1b,c); however, on the transcriptional level, high expression of both uPA and PAI1 showed a significantly decreased OS (Supplementary Figure S1d,e).

3.2. Generation of CRISPR/Cas9 uPAR Knockout Clones in AsPC-1 Cells

Next, we wanted to investigate the molecular function of uPAR in PDAC cells. Therefore, we measured the uPAR protein expression levels by ELISA in six PDAC cell lines with known gene mutation status of *KRAS*, *TP53*, and *PIK3CA* as described in the Material and Methods section (Supplementary Figure S2a,b and Supplementary Table S1). We then generated *uPAR* knockout clones of the cell line with the highest uPAR expression (AsPC-1), using two gRNAs directed against *uPAR* exons 3 and 4 (Supplementary Figure S2c). Two clones with homozygous functional *uPAR* knockout (KO#1 and KO#2), carrying a deletion on one allele and a gRNA target-site-specific frameshift mutation on the other, revealed a virtually absent uPAR protein (Supplementary Figure S2d–g).

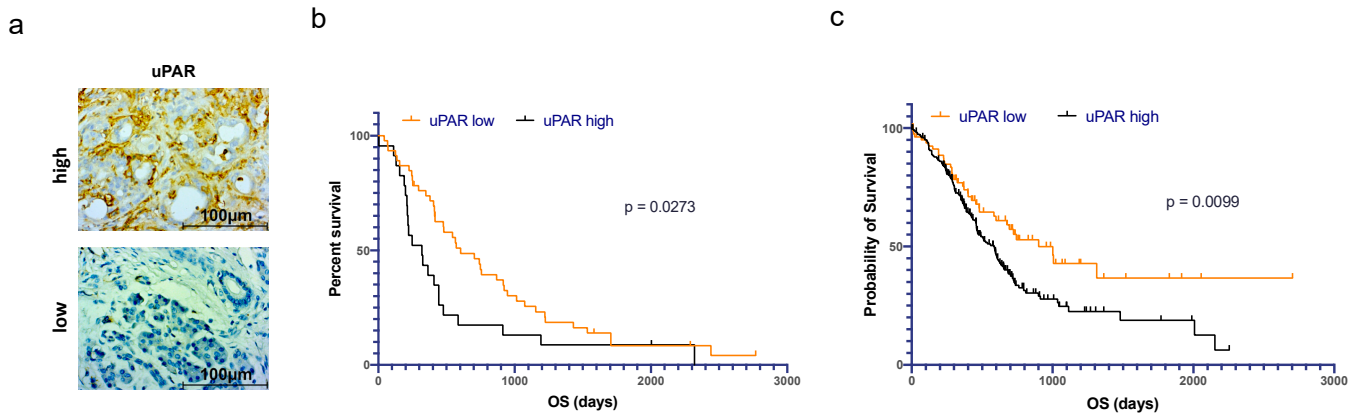


Figure 1. Prognostic significance of uPAR expression in PDAC patients. (a) Exemplary immunohistochemical staining of PDAC with high vs. low expression of uPAR. (b) Statistically significant difference in OS for $n = 67$ PDAC patients with high (orange, $n = 45$) vs. low (black, $n = 22$) immunohistochemical expression of uPAR. (c) Statistically significant difference in OS for $n = 83$ PDAC patients with high (black) vs. $n = 219$ patients with low (orange) expression levels of uPAR mRNA (source: TCGA dataset).

3.3. uPAR Influences Cell Growth, Cellular Plasticity, and the Response to Gemcitabine in AsPC-1 (*KRAS^{G12D}*)

Functional roles of uPAR have been described in cell proliferation, migration, and cellular plasticity [28–31]. Both AsPC-1 *uPAR*^{-/-} clones showed a significant decrease in growth and migration capacity compared to the AsPC-1 WT controls (Figure 2a,b). To evaluate the role of uPAR in cellular plasticity, we immunoblotted nine markers involved in epithelial–mesenchymal transition (EMT) (Figure 2c).

Western blot revealed a marked upregulation of epithelial markers E-cadherin and β -catenin. While the transcription factor Slug was slightly upregulated, Snail and TCF8/ZEB1, together with claudin and ZO1, showed a decreased expression, further indicating the mesenchymal to epithelial transition (MET) in *uPAR*^{-/-} clones compared to AsPC-1 WT (Figure 2c). In accordance with this phenotype, we detected a marked increase in chemoresistance against up to 1 μ M gemcitabine in *uPAR*^{-/-} cells (Figure 2d).

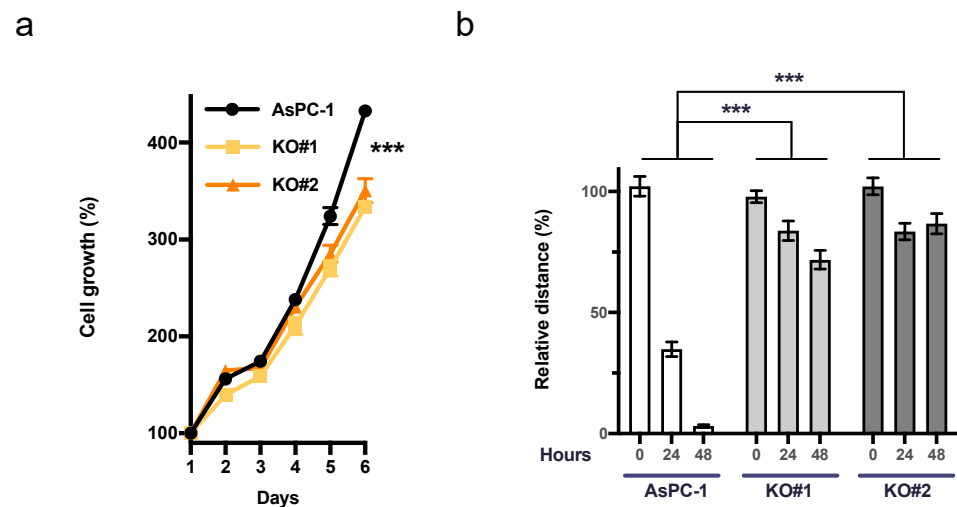


Figure 2. Cont.

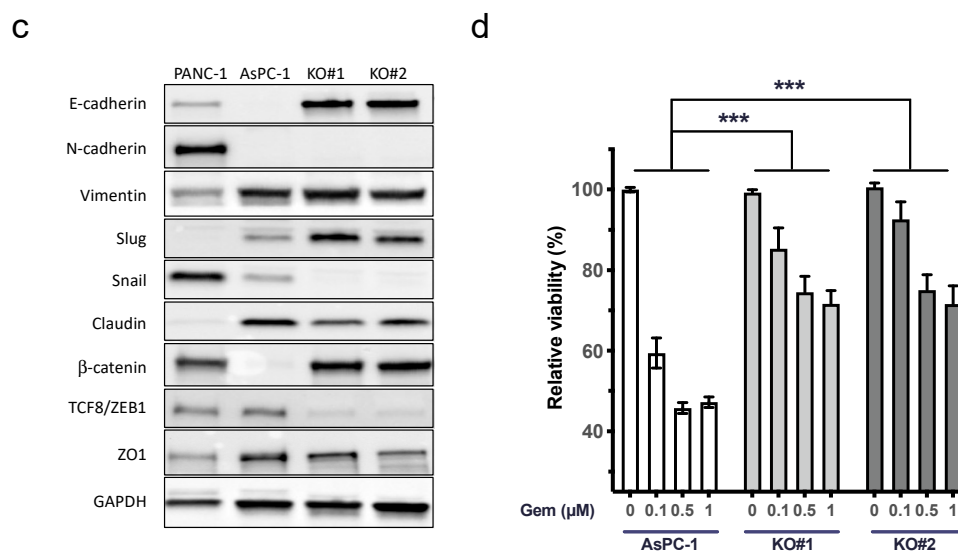


Figure 2. Decreased cell growth, motility, and response to gemcitabine of AsPC uPAR knockout clones. (a) Cell growth analysis (6 days) of $uPAR^{-/-}$ clones with a significantly slower proliferation rate than WT controls ($n = 3$). (b) Reduced migratory capacity of AsPC-1 $uPAR^{-/-}$ clones compared to $uPAR^{WT}$ cells ($n = 3$). (c) Western blot analysis of 9 epithelial and mesenchymal markers in PANC-1, AsPC-1, and $uPAR^{-/-}$ clones indicated *mesenchymal to epithelial transition* (MET) in $uPAR^{-/-}$ cells. Uncropped Western blot images available in Supplementary Material File S1 (d) Increased resistance of $uPAR^{-/-}$ clones to gemcitabine treatment (0.1, 0.5 and 1 μ M) for 72 h ($n = 4$ biological replicates). (KO#1 and KO#2, $uPAR^{-/-}$ clones) (** $p < 0.001$).

3.4. Depletion of uPAR Activates FAK, CDC42, and p38 and Induces Autophagy

uPAR signaling has been described to involve FAK, Src, CDC42, p38, autophagy, and RAS signaling [32]. In addition, Wu et al. reported that FAK signaling contributes to intrinsic gemcitabine chemoresistance in pancreatic cancer cell lines [33]. By immunoblotting, we detected the activation of FAK, CDC42, p38, and LC3B, while ERK was inactivated in AsPC-1 $uPAR^{-/-}$ cells (Figure 3a). The influence of FAK on Ras signaling has been described before [34]. However, in cells with aberrant KRAS activation, FAK-Ras regulation seems to be disturbed.

Knockdown of FAK in $uPAR^{-/-}$ cells using siRNAs led to decreased phosphorylation of CDC42, p38, and LC3B, and reactivation of ERK (Figure 3b). The diminished FAK activity also partially restored the sensitivity towards gemcitabine (Figure 3c and Supplementary Figure S3a). Knockdown of CDC42 and p38 also reactivated ERK, decreased LC3B, and increased gemcitabine sensitivity (Figure 3d–g and Supplementary Figure S3b,c). This indicates that CDC42 and p38 suppress ERK activity downstream of KRAS in the absence of uPAR.

3.5. Re-expression of uPAR Restores the Migratory Capability and Gemcitabine Sensitivity of $uPAR^{-/-}$ Cells

To evaluate whether uPAR re-expression could restore the WT phenotype, $uPAR^{-/-}$ cells were transfected with a human uPAR gene expression vector as described in the Material and Methods section. This recovered uPAR protein levels (Supplementary Figure S2h) and significantly enhanced migratory capacity (Figure 3h). uPAR re-expression also recovered gemcitabine sensitivity and induced resistance against the p38 inhibitor JX401 (Figure 3i and Supplementary Figure S3d). Pharmacological inhibition of ERK with SCH772948 reduced gemcitabine sensitivity only in uPAR WT but not in AsPC-1 $uPAR^{-/-}$ cells (Figure 3j and Supplementary Figure S3e). Together, this indicates that uPAR mediates gemcitabine sensitivity in an ERK-dependent manner.

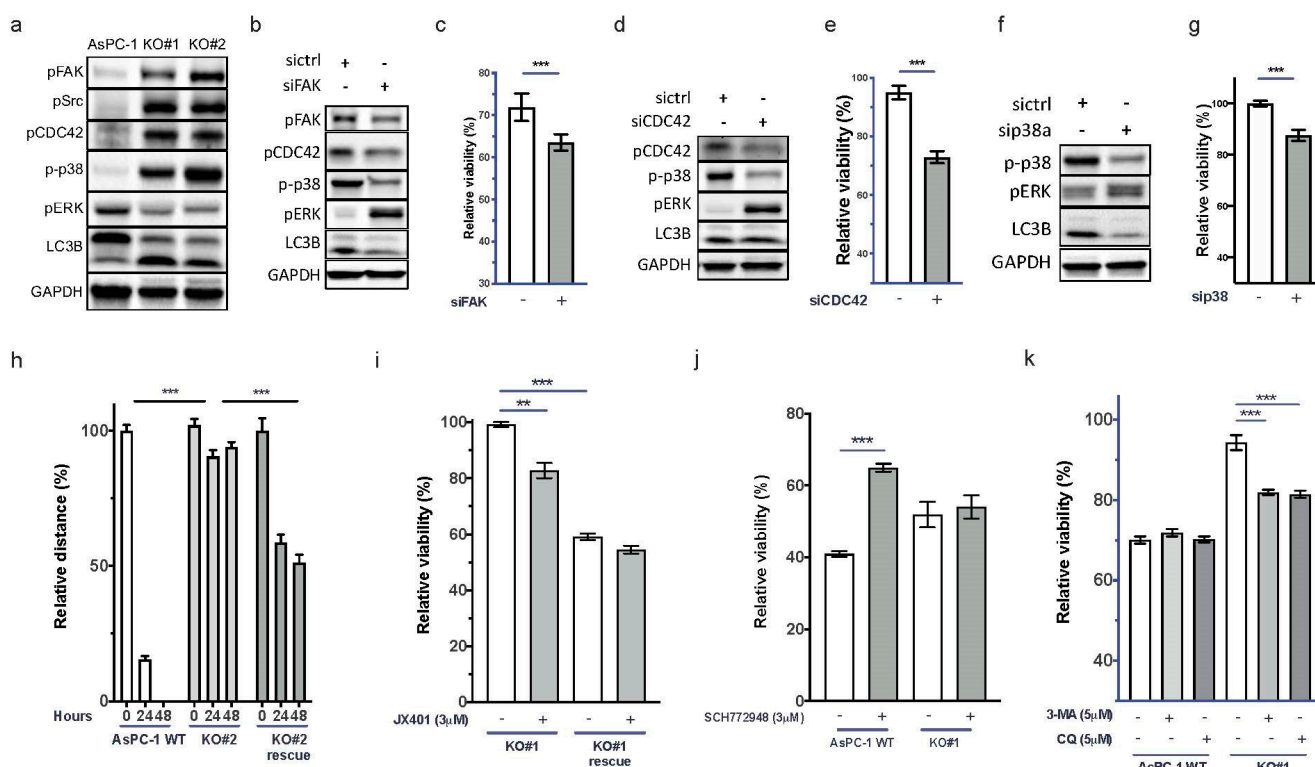


Figure 3. uPAR regulates CDC42, p38, LC3B, and ERK activity. (a) Immunoblot showing increased signals for pCDC42, pSrc, p-p38, pERK, and LC3B in KO#1 and KO#2. (b) Uncropped Western blot images could be found at in Supplementary File S1. Restoration of (b) the wild-type signaling phenotype after FAK siRNA knockdown in AsPC-1 *uPAR*^{-/-} cells and (c) of the response to gemcitabine ($n = 4$). Uncropped Western blot images could be found at in Supplementary File S1 (d) Knockdown of CDC42 by siRNA and (e) response to gemcitabine and (f) siRNA knockdown of p38 and (g) the corresponding gemcitabine response. Uncropped Western blot images available in Supplementary File S1. (h) Increased cellular motility after transient uPAR expression in KO#2 (KO#2 rescue) compared to AsPC-1 *uPAR*^{-/-} cells ($n = 4$). (i) Gemcitabine (0.1 μM) and combinational treatment with the p38 inhibitor JX401 for 72 h in AsPC-1 *uPAR*^{-/-} and KO#1 uPAR rescue cells ($n = 3$). (j) Gemcitabine (0.1 μM) and combinational treatment with the ERK inhibitor SCH772948 in uPAR WT and AsPC-1 *uPAR*^{-/-} cells (KO#1). (k) Treatment of AsPC-1 WT and AsPC-1 *uPAR*^{-/-} (KO#1) with either gemcitabine (0.1 μM) or in combination with the autophagy inhibitors 3-MA (5 μM) or CQ (5 μM). Relative viability is shown in response to gemcitabine and in combination with siRNA/inhibitors. ($n = 4$ biological replicates (** $p < 0.01$, *** $p < 0.001$)).

3.6. Resistance against Gemcitabine in AsPC-1 *uPAR*^{-/-} Cells through Autophagy

The autophagy marker LC3B was induced in AsPC-1 *uPAR*^{-/-} cells. Autophagy promotes tumor cell survival and contributes to chemoresistance [35]. Increased autophagy has been described to be responsible for the resistance of PDAC to gemcitabine that could be partially reversed by specific inhibitors [36]. To investigate whether increased autophagy in *uPAR*^{-/-} clones was responsible for the observed gemcitabine resistance, we inhibited autophagy with 3-methyladenine (3-MA) or chloroquine (CQ). Both inhibitors significantly restored sensitivity towards gemcitabine in AsPC-1 *uPAR*^{-/-} but not in AsPC-1 WT (Figure 3k and Supplementary Figure S3f).

3.7. uPAR and Mutated KRAS Cooperate in Maintaining a Mesenchymal Phenotype

To evaluate the interplay of uPAR and mutated *KRAS* in response to gemcitabine, we used the *KRAS* WT cell line BxPC-3 (uPAR high), the *KRAS* mutant cell line AsPC1 (uPAR high), and the *KRAS* mutant cell line PANC-1 (uPAR low) (Figure 4a and Supplementary Figure S2a).

AsPC1 responded best towards gemcitabine, PANC-1 showed a medium response, and BxPC3 was the most resistant cell line (Figure 4b). *KRAS* has been described to induce uPAR expression [17]. Silencing of *KRAS* in AsPC1 using siRNAs reduced uPAR levels significantly (Figure 4c). Silencing of *KRAS* in AsPC1 reduced the response towards gemcitabine whereas the expression of mutated *KRAS* in BxPC-3 cells increased gemcitabine sensitivity. Transfection of uPAR in PANC-1 likewise increased gemcitabine sensitivity (Figure 4d). uPAR and mutated *KRAS* switched cells to a mesenchymal phenotype (Figure 4e), at the same time promoting activation of MEK and ERK and suppressing FAK and CDC42 signaling (Figure 4f).

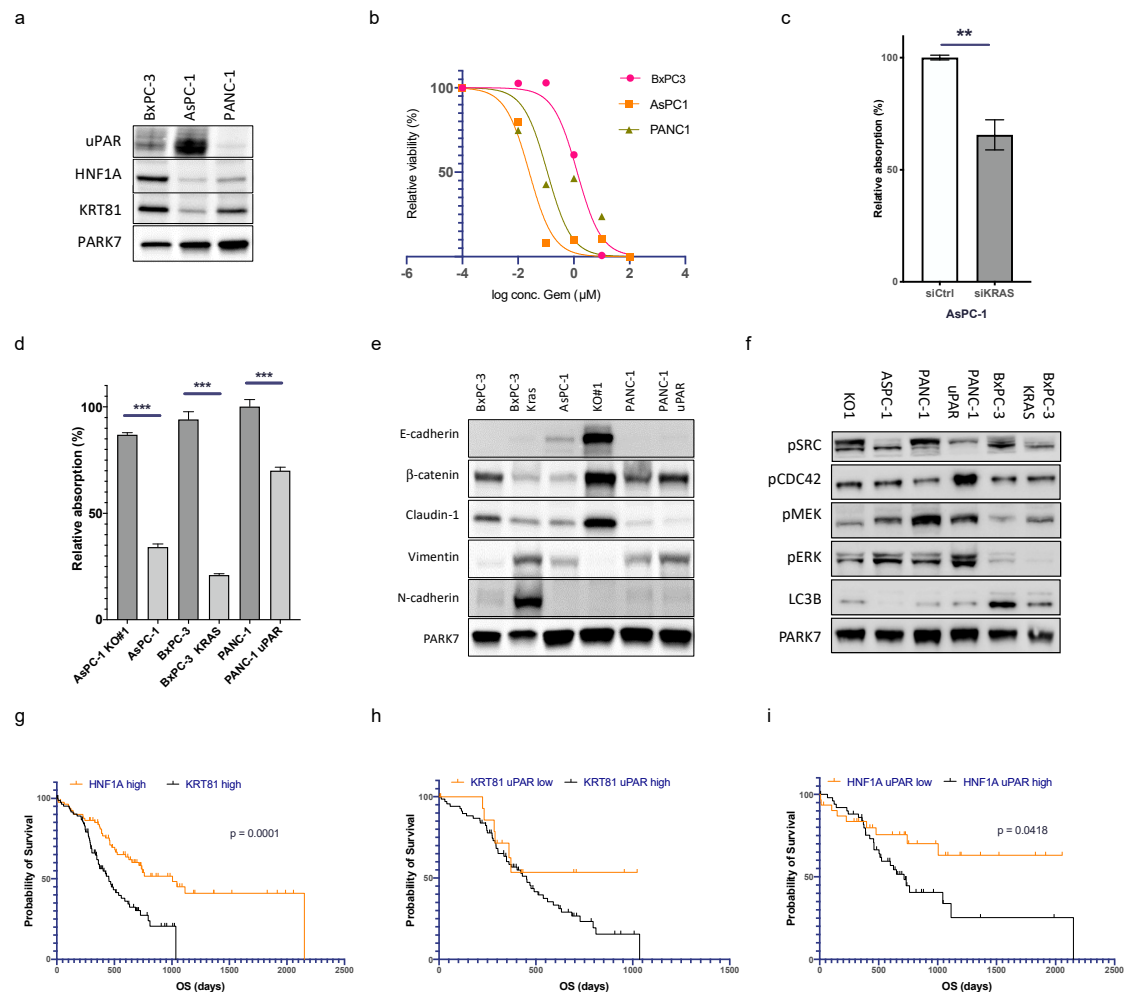


Figure 4. uPAR and mutated *KRAS* cooperate in maintaining a mesenchymal phenotype that also regulates gemcitabine sensitivity. (a) Immunoblot showing uPAR, HNF1A, and KRT81 expression in BxPC-3, AsPC-1, and PANC-1. Uncropped Western blot images available in Supplementary File S1 (b) IC₅₀ of gemcitabine treatment (0–100 μM, 72 h) in BxPC-3 (1.323 μM), AsPC-1 (0.025 μM), and PANC-1 (0.112 μM). (c) uPAR levels after *KRAS* siRNA knockdown in AsPC-1 ($n = 3$ biological replicates, ** Student's t -test, $p < 0.01$, *** Student's t -test, $p < 0.001$). (d) Gemcitabine response (0.125 μM, 72 h) in AsPC-1 WT, AsPC-1 *uPAR*^{-/-} (KO#1), BxPC-3 (*KRAS* WT), BxPC-3 (*KRAS*^{mut}), PANC-1 (*uPAR*^{low}), and PANC-1 (*uPAR*^{high}). (e) Immunoblot of protein lysates from the same cell lines for EMT markers and (f) pFAK, pCDC42, p-p38, pMEK, p-ERK, and LC3B. Kaplan–Meier curves using mRNA expression data of PDAC from the TCGA cohort. Uncropped Western blot images available in Supplementary File S1. (g) Comparison of PDAC with high expression of *HNF1A* vs. *KRT81*. (h) *KRT81*^{high} tumors with high vs. low expression of *uPAR* and (i) *HNF1A*^{high} tumors with high vs. low expression of *uPAR* (log-rank test, $p < 0.05$).

3.8. uPAR Modulates the Clinical Risk in Different PDAC Subgroups

Noll et al. [8] published HNF1A as a surrogate marker for the exocrine-like PDAC subtype and expression of keratin 81 (KRT81) as a marker for the quasi-mesenchymal (QM) type. Tumors negative for both markers (DN) were enriched for the classical PDAC subtype. We wanted to know if tumors with high uPAR expression segregate with one of these subtypes. In our own cohort of 57 patients with clinical follow-up, $n = 31$ (54%) showed expression of HNF1A, $n = 19$ (33%) were positive for KRT81, and $n = 7$ (12%) were DN. Because the DN group was too small, we excluded it from further analysis. The exocrine-like group consisted of 21 uPAR low and 10 uPAR high cases, and the QM group contained 9 uPAR low and 10 uPAR high cases. Survival analysis was supplemented by gene expression data from the two TCGA cohorts ($n = 82$ cases HNF1A high vs. $n = 85$ cases KRT81 high).

The overall survival of patients with HNF1A-positive exocrine-like PDAC was significantly longer than patients with KRT81-positive QM tumors ($p < 0.0001$, Figure 4g). In the HNF1A-positive cohort, tumors with low levels of uPAR had a significantly better outcome than tumors with high expression and the mortality curve even reached a plateau after 1000 days, indicating long-term survival of some patients. In the KRT81^{high} QM and DN group, there was a trend towards longer survival in patients with tumors with low levels of uPAR that did not reach statistical significance (Figure 4h,i and Supplementary Figure S4), indicating that the prognostic impact of uPAR may vary among different molecular subgroups.

4. Discussion

PDAC remains one of the human tumors with the highest mortality. uPAR is associated with early invasion, metastasis, and poor prognosis in many solid and hematological tumors [9–11]. We have previously shown that PDAC with high-level gene amplifications of *uPAR* have a particularly poor prognosis [24]. We here show in our cohort of 67 samples and in 168 PDAC samples from the TCGA database that overexpression of uPAR on the mRNA and protein level is also associated with significantly shorter OS. Importantly, although our data suggest that high expression of uPAR is an adverse prognostic factor in all PDAC, its negative impact on survival is more pronounced in some molecular subgroups (especially in exocrine-like tumors) than in others.

uPAR has been described to act through its vitronectin-mediated interaction with integrins to transmit mechanical forces across the cell membrane [37–39]. The ECM–integrin interaction mediates the intrinsic chemoresistance of cancer cells [40], a phenomenon that has also been called cell-adhesion-mediated drug resistance (CMDR). CMDR has been explained by the strong binding of integrins to the ECM, which activates FAK. Integrin and EGFR signaling activates FAK and influences adhesion, motility, and cell growth [41,42]. FAK has seemingly paradoxical roles in cell migration and metastasis [43]. FAK is a ubiquitously expressed tyrosine kinase that localizes at focal adhesion complexes and transmits adhesion- and growth-factor-dependent signals into the cell [34,43,44]. In contrast to normal cells where FAK is a positive regulator of cell migration and proliferation [45], tumors with constitutive growth factor signaling (such as EGFR) or *RAS* mutations and consecutive high intrinsic levels of ERK utilize FAK as a negative regulator of cell migration through ERK-dependent dephosphorylation of particular FAK tyrosine residues [43,46]. Constitutive activation of FAK has also been proposed to contribute to the intrinsic chemoresistance against gemcitabine in the pancreatic cancer cell line AsPC-1 [9,33]. We here show that uPAR knockout in AsPC1 cells leads to induction of FAK, Src, CDC42, and p38, as well as chemoresistance towards gemcitabine. Our data further show that this chemoresistance is mediated through p38-induced autophagy. Numerous early clinical trials [47] have shown significant antitumor activity with tolerable toxicity of the autophagy inhibitor chloroquine, in combination with other cytotoxic chemotherapies in a variety of solid cancers, including colorectal and renal cell carcinomas [48]. A randomized clinical phase II trial in 102 PDAC patients treated with gemcitabine and nab-paclitaxel with or without CQ showed no differ-

ence in progression-free survival. Still, the authors proposed that preoperative CQ might increase curative resection rates [49].

A total of 90–95% of PDACs harbor activating mutations of *KRAS* that are thought to occur early in carcinogenesis [16]. Mutated *KRAS* is a potent oncogenic driver that promotes cell proliferation and migration by activating the downstream MAP kinases ERK1/2 [50]. *KRAS* has not only been reported to induce uPAR expression by AP-1-dependent transactivation of the *uPAR* promoter [17], but also mediates FAK dephosphorylation [43]. We here show that a) constitutively active *KRAS* induces uPAR and b) *KRAS* and uPAR cooperate in promoting a mesenchymal cell phenotype by activating MEK/ERK signaling and by the suppression of FAK/CDC42/p38 signaling. At the cellular level, this mesenchymal state implies increased cell proliferation and migration as a possible explanation of the poor prognosis of tumors with high levels of uPAR. At the same time, it also implies suppressed cellular dormancy via FAK signaling and p38-mediated autophagy, thus rendering the cells more vulnerable to gemcitabine. These observations highlight a potential therapeutic dilemma that applies both to *KRAS* and uPAR as emerging targets. Although recent studies propose uPAR as a good candidate for antibody-targeted therapy in cancer [51–55], our results show that these treatments could, at the same time, induce cellular dormancy and render the tumor more resistant to chemotherapy (such as gemcitabine). Tailored strategies should consider this resistance by adding autophagy inhibitors, such as chloroquine, to the regimens.

5. Conclusions

In summary, we have confirmed uPAR as a potent modulating prognostic factor, especially in the large molecular subgroup of exocrine-like tumors. uPAR cooperates with mutated *KRAS* in the important switch between an active mesenchymal vs. a dormant epithelial cellular phenotype. By keeping tumor cells in the active mesenchymal state, uPAR promotes *KRAS*-driven proliferation and cell migration as a likely explanation for the poor prognosis of PDAC with high expression of uPAR. At the same time, this active mesenchymal state renders tumor cells more vulnerable to chemotherapy such as gemcitabine. Targeting either uPAR or *KRAS* could induce cellular dormancy and autophagy, thus leading to relative chemoresistance and limited therapeutic efficacy. Emerging clinical trials should take this possibility into account.

Supplementary Materials: The following supporting information can be downloaded at: <https://www.mdpi.com/article/10.3390/cancers15051587/s1>, Supplementary Figure S1: (a) Staining intensities (300 score) of uPA, uPAR, and PAI1 of 69 PDAC patient samples. (b) OS analysis of PDAC patients with low vs. high protein expression of uPA on immunohistochemistry, and (c) PAI1. (d) OS analysis of PDAC patients with low vs. high mRNA expression of uPA (Cox-Mantel-test, $p = 0.0475$) and (e) PAI1; Supplementary Figure S2: (a) uPAR and (b) uPA protein levels of the pancreatic cell lines AsPC-1, BxPC-3, CAPAN-2, MIA PaCa-2, PATU8988T, and PANC-1 measured by ELISA. (c) Schematic representation of the uPAR CRISPR/Cas9 strategy. Two gRNAs were directed against exon three and exon 4 of the uPAR gene and were used to generate uPAR^{-/-} clones. (d–f) Sanger sequencing analysis of two uPAR^{-/-} clones consisting of a large deletion and a site-specific mutation. (g) ELISA measurement of uPAR levels in KO#1 and KO#2 compared to uPAR WT and (h) of rescue KO#2 by re-expressing uPAR compared to KO#2. (i) Exemplary pictures of the migration assay of AsPC-1 WT, KO#1 and KO#2 over 48 h; Supplementary Figure S3: Gemcitabine treatment after siRNA knockdown and p38 inhibition in AsPC1 WT and uPAR^{-/-} cells. Gemcitabine response (0.1 μM, 72 h) after siRNA knockdown (80 nM, 24 h) of (a) FAK, (b) CDC42 and (c) of p38 in AsPC1 KO#2. (d) Gemcitabine treatment of AsPC-1 WT and uPAR^{-/-} cells (KO#2) in combination with the p38 inhibitor JX401. (e) Gemcitabine treatment (0.1 μM, 72 h) vs. combination with ERK inhibition (SCH772948, 3 μM) of uPAR^{-/-} cells (KO#2). (f) Treatment of uPAR knock-out clones (KO#2) with either gemcitabine (0.1 μM) or in combination with the autophagy inhibitors 3-MA (5 μM) or CQ (5 μM) ($n = 4$); Supplementary Figure S4: Kaplan Meyer OS analysis of TCGA patient cohort. (a) uPAR low ($n = 15$) vs. uPAR high ($n = 49$) in DN cases and (b) uPAR low ($n = 22$) vs. uPAR high ($n = 69$) in DP cases; Table S1; Human PDAC cell lines with TP53 and *KRAS* mutation status; Table S2:

siRNAs (Qiagen); Table S3: Antibodies and chemicals; Supplementary Material File S1: Uncropped WB images.

Author Contributions: Conceptualization, S.K., L.P. and P.S.; data curation, S.K., L.P., Y.L., S.Y., J.K., V.M.B., C.F.M.S., F.F. and H.B.; formal analysis, S.K., L.P., Y.L., J.K., V.M.B., C.F.M.S., F.F. and H.B.; investigation, S.K., Y.L. and L.P.; methodology, S.K. and L.P.; project administration, S.K., L.P. and P.S.; resources, J.G., A.N., V.E. and P.S.; supervision, S.K. and P.S.; visualization, S.K.; writing—original draft, S.K., L.P. and P.S.; writing—review and editing, S.K. and P.S. All authors have read and agreed to the published version of the manuscript.

Funding: P.S. is supported by the Deutsche Forschungsgemeinschaft (KFO5002). L.P. received funding from the Hunan Provincial Health Committee Foundation of China (Grant No. D202302087111).

Institutional Review Board Statement: The study was conducted according to the guidelines of the Declaration of Helsinki and approved by the Ethics Committee of the University Medical Center Göttingen (GÖ 912/15).

Informed Consent Statement: Written informed consent for the clinical procedure was obtained from all participants.

Data Availability Statement: The data presented in this study are available in the article, the Supplementary Materials and at TCGA (<https://www.cbioportal.org>, accessed on 30 January 2023: Pancreatic Adenocarcinoma, Firehose Legacy and PanCancer Atlas).

Acknowledgments: We thank Ulrike Ehbrecht, Jennifer Appelhans, Monique Küffer, and Stefanie Schwager for their excellent technical support.

Conflicts of Interest: The authors declare no conflict of interest.

References

1. Kindler, H.L. A Glimmer of Hope for Pancreatic Cancer. *N. Engl. J. Med.* **2018**, *379*, 2463–2464. [[CrossRef](#)]
2. Nevala-Plagemann, C.; Hidalgo, M.; Garrido-Laguna, I. From state-of-the-art treatments to novel therapies for advanced-stage pancreatic cancer. *Nat. Rev. Clin. Oncol.* **2020**, *17*, 108–123. [[CrossRef](#)] [[PubMed](#)]
3. Conroy, T.; Desseigne, F.; Ychou, M.; Bouché, O.; Guimbaud, R.; Bécouarn, Y.; Adenis, A.; Raoul, J.-L.; Gourgou-Bourgade, S.; De La Fouchardière, C.; et al. FOLFIRINOX versus Gemcitabine for Metastatic Pancreatic Cancer. *N. Engl. J. Med.* **2011**, *364*, 1817–1825. [[CrossRef](#)] [[PubMed](#)]
4. Von Hoff, D.D.; Ervin, T.; Arena, F.P.; Chiorean, E.G.; Infante, J.; Moore, M.; Seay, T.; Tjulandin, S.A.; Ma, W.W.; Saleh, M.N.; et al. Increased survival in pancreatic cancer with nab-paclitaxel plus gemcitabine. *N. Engl. J. Med.* **2013**, *369*, 1691–1703. [[CrossRef](#)]
5. van Roessel, S.; Kasumova, G.G.; Verheij, J.; Najarian, R.M.; Maggino, L.; de Pastena, M.; Malleo, G.; Marchegiani, G.; Salvia, R.; Ng, S.C.; et al. International Validation of the Eighth Edition of the American Joint Committee on Cancer (AJCC) TNM Staging System in Patients With Resected Pancreatic Cancer. *JAMA Surg.* **2018**, *153*, e183617. [[CrossRef](#)]
6. Collisson, E.A.; Sadanandam, A.; Olson, P.; Gibb, W.J.; Truitt, M.; Gu, S.; Cooc, J.; Weinkle, J.; Kim, G.E.; Jakkula, L.; et al. Subtypes of pancreatic ductal adenocarcinoma and their differing responses to therapy. *Nat. Med.* **2011**, *17*, 500–503. [[CrossRef](#)]
7. Patil, S.; Steuber, B.; Kopp, W.; Kari, V.; Urbach, L.; Wang, X.; Küffer, S.; Bohnenberger, H.; Spyropoulou, D.; Zhang, Z.; et al. EZH2 Regulates Pancreatic Cancer Subtype Identity and Tumor Progression via Transcriptional Repression of GATA6. *Cancer Res.* **2020**, *80*, 4620–4632. [[CrossRef](#)] [[PubMed](#)]
8. Noll, E.M.; Eisen, C.; Stenzinger, A.; Espinet, E.; Muckenhuber, A.; Klein, C.; Vogel, V.; Klaus, B.; Nadler, W.; Rösli, C.; et al. CYP3A5 mediates basal and acquired therapy resistance in different subtypes of pancreatic ductal adenocarcinoma. *Nat. Med.* **2016**, *22*, 278–287. [[CrossRef](#)]
9. Jacobsen, B.; Ploug, M. The urokinase receptor and its structural homologue C4.4A in human cancer: Expression, prognosis and pharmacological inhibition. *Curr. Med. Chem.* **2008**, *15*, 2559–2573. [[CrossRef](#)]
10. Morten, G.R.; Rasch, M.G.; Lund, I.K.; Almasi, C.E.; Hoyer-Hansen, G. Intact and cleaved uPAR forms: Diagnostic and prognostic value in cancer. *Front. Biosci.* **2008**, *13*, 6752–6762. [[CrossRef](#)]
11. Béné, M.C.; Castoldi, G.; Knapp, W.; Rigolin, G.M.; Escribano, L.; Lemez, P.; Ludwig, W.-D.; Matutes, E.; Orfao, A.; Lanza, F.; et al. CD87 (urokinase-type plasminogen activator receptor), function and pathology in hematological disorders: A review. *Leukemia* **2004**, *18*, 394–400. [[CrossRef](#)] [[PubMed](#)]
12. Montuori, N.; Cosimato, V.; Rinaldi, L.; Rea, V.E.; Alfano, D.; Ragno, P. uPAR regulates pericellular proteolysis through a mechanism involving integrins and fMLF-receptors. *Thromb. Haemost.* **2013**, *109*, 309–318.
13. Tang, C.-H.; Wei, Y. The urokinase receptor and integrins in cancer progression. *Cell. Mol. Life Sci.* **2008**, *65*, 1916–1932. [[CrossRef](#)] [[PubMed](#)]

14. Madsen, D.H.; Engelholm, L.H.; Ingvarsen, S.; Hillig, T.; Wagenaar-Miller, R.A.; Kjølner, L.; Gårdsvoll, H.; Høyer-Hansen, G.; Holmbeck, K.; Bugge, T.H.; et al. Extracellular Collagenases and the Endocytic Receptor, Urokinase Plasminogen Activator Receptor-associated Protein/Endo180, Cooperate in Fibroblast-mediated Collagen Degradation. *J. Biol. Chem.* **2007**, *282*, 27037–27045. [[CrossRef](#)] [[PubMed](#)]
15. Smith, H.W.; Marshall, C.J. Regulation of cell signalling by uPAR. *Nat. Rev. Mol. Cell Biol.* **2010**, *11*, 23–36. [[CrossRef](#)]
16. Yang, K.; Li, Y.; Lian, G.; Lin, H.; Shang, C.; Zeng, L.; Chen, S.; Li, J.; Huang, C.; Huang, K.; et al. KRAS promotes tumor metastasis and chemoresistance by repressing RKIP via the MAPK-ERK pathway in pancreatic cancer. *Int. J. Cancer* **2018**, *142*, 2323–2334. [[CrossRef](#)]
17. Allgayer, H.; Wang, H.; Shirasawa, S.; Sasazuki, T.; Boyd, D. Targeted disruption of the K-Ras oncogene in an invasive colon cancer cell line down-regulates urokinase receptor expression and plasminogen-dependent proteolysis. *Br. J. Cancer* **1999**, *80*, 1884–1891. [[CrossRef](#)]
18. Kren, A.; Baeriswyl, V.; Lehembre, F.; Wunderlin, C.; Strittmatter, K.; Antoniadis, H.; Fässler, R.; Cavallaro, U.; Christofori, G. Increased tumor cell dissemination and cellular senescence in the absence of beta1-integrin function. *EMBO J.* **2007**, *26*, 2832–2842. [[CrossRef](#)]
19. Liu, D.; Ghiso, J.A.; Estrada, Y.; Ossowski, L. EGFR is a transducer of the urokinase receptor initiated signal that is required for in vivo growth of a human carcinoma. *Cancer Cell* **2002**, *1*, 445–457. [[CrossRef](#)]
20. Hildenbrand, R.; Allgayer, H.; Marx, A.; Stroebel, P. Modulators of the urokinase-type plasminogen activation system for cancer. *Expert Opin. Investig. Drugs* **2010**, *19*, 641–652. [[CrossRef](#)]
21. Budczies, J.; Klauschen, F.; Sinn, B.V.; Györffy, B.; Schmitt, W.D.; Darb-Esfahani, S.; Denkert, C. Cutoff Finder: A Comprehensive and Straightforward Web Application Enabling Rapid Biomarker Cutoff Optimization. *PLoS ONE* **2012**, *7*, e51862. [[CrossRef](#)] [[PubMed](#)]
22. Li, Y.; Elakad, O.; Yao, S.; von Hammerstein-Equord, A.; Hinterthaler, M.; Danner, B.C.; Ferrai, C.; Ströbel, P.; Küffer, S.; Bohnenberger, H. Regulation and Therapeutic Targeting of MTHFD2 and EZH2 in KRAS-Mutated Human Pulmonary Adenocarcinoma. *Metabolites* **2022**, *12*, 652. [[CrossRef](#)]
23. Müller, D.; Mazzeo, P.; Koch, R.; Boshertz, M.S.; Welter, S.; von Hammerstein-Equord, A.; Hinterthaler, M.; Cordes, L.; Belharazem, D.; Marx, A.; et al. Functional apoptosis profiling identifies MCL-1 and BCL-xL as prognostic markers and therapeutic targets in advanced thymomas and thymic carcinomas. *BMC Med.* **2021**, *19*, 300. [[CrossRef](#)]
24. Hildenbrand, R.; Niedergethmann, M.; Marx, A.; Belharazem, D.; Allgayer, H.; Schleger, C.; Ströbel, P. Amplification of the Urokinase-Type Plasminogen Activator Receptor (uPAR) Gene in Ductal Pancreatic Carcinomas Identifies a Clinically High-Risk Group. *Am. J. Pathol.* **2009**, *174*, 2246–2253. [[CrossRef](#)]
25. de Geus, S.W.; Baart, V.M.; Boonstra, M.C.; Kuppen, P.J.; Prevoo, H.A.; Mazar, A.P.; Bonsing, B.A.; Morreau, H.; van de Velde, C.J.; Vahrmeijer, A.L.; et al. Prognostic Impact of Urokinase Plasminogen Activator Receptor Expression in Pancreatic Cancer: Malignant Versus Stromal Cells. *Biomark Insights* **2017**, *12*, 1177271917715443. [[CrossRef](#)]
26. Cao, L.; Huang, C.; Cui Zhou, D.; Hu, Y.; Lih, T.M.; Savage, S.R.; Krug, K.; Clark, D.J.; Schnaubelt, M.; Chen, L.; et al. Proteogenomic characterization of pancreatic ductal adenocarcinoma. *Cell* **2021**, *184*, 5031–5052.e26. [[CrossRef](#)]
27. Hoadley, K.A.; Yau, C.; Hinoue, T.; Wolf, D.M.; Lazar, A.J.; Drill, E.; Shen, R.; Taylor, A.M.; Cherniack, A.D.; Thorsson, V.; et al. Cell-of-Origin Patterns Dominate the Molecular Classification of 10,000 Tumors from 33 Types of Cancer. *Cell* **2018**, *173*, 291–304.e6. [[CrossRef](#)] [[PubMed](#)]
28. Aguirre-Ghiso, J.A.; Liu, D.; Mignatti, A.; Kovalski, K.; Ossowski, L. Urokinase receptor and fibronectin regulate the ERK(MAPK) to p38(MAPK) activity ratios that determine carcinoma cell proliferation or dormancy in vivo. *Mol. Biol. Cell* **2001**, *12*, 863–879. [[CrossRef](#)] [[PubMed](#)]
29. Smith, H.W.; Marra, P.; Marshall, C.J. uPAR promotes formation of the p130Cas–Crk complex to activate Rac through DOCK180. *J. Cell Biol.* **2008**, *182*, 777–790. [[CrossRef](#)] [[PubMed](#)]
30. Lester, R.D.; Jo, M.; Montel, V.; Takimoto, S.; Gonias, S.L. uPAR induces epithelial–mesenchymal transition in hypoxic breast cancer cells. *J. Cell Biol.* **2007**, *178*, 425–436. [[CrossRef](#)] [[PubMed](#)]
31. Jo, M.; Lester, R.D.; Montel, V.; Eastman, B.; Takimoto, S.; Gonias, S.L. Reversibility of Epithelial-Mesenchymal Transition (EMT) Induced in Breast Cancer Cells by Activation of Urokinase Receptor-dependent Cell Signaling. *J. Biol. Chem.* **2009**, *284*, 22825–22833. [[CrossRef](#)] [[PubMed](#)]
32. Santibanez, J.F. Transforming Growth Factor-Beta and Urokinase-Type Plasminogen Activator: Dangerous Partners in Tumorigenesis—Implications in Skin Cancer. *ISRN Dermatol.* **2013**, *2013*, 597927. [[CrossRef](#)] [[PubMed](#)]
33. Huanwen, W.; Zhiyong, L.; Xiaohua, S.; Xinyu, R.; Kai, W.; Tonghua, L. Intrinsic chemoresistance to gemcitabine is associated with constitutive and laminin-induced phosphorylation of FAK in pancreatic cancer cell lines. *Mol. Cancer* **2009**, *8*, 125. [[CrossRef](#)] [[PubMed](#)]
34. Barkan, D.; Chambers, A.F. Beta1-integrin: A potential therapeutic target in the battle against cancer recurrence. *Clin. Cancer Res.* **2011**, *17*, 7219–7223. [[CrossRef](#)]
35. Levy, J.M.M.; Towers, C.G.; Thorburn, A. Targeting autophagy in cancer. *Nat. Rev. Cancer* **2017**, *17*, 528–542. [[CrossRef](#)]
36. Bryant, K.L.; Stalneck, C.A.; Zeitouni, D.; Klomp, J.E.; Peng, S.; Tikunov, A.P.; Gunda, V.; Pierobon, M.; Waters, A.M.; George, S.D.; et al. Combination of ERK and autophagy inhibition as a treatment approach for pancreatic cancer. *Nat. Med.* **2019**, *25*, 628–640. [[CrossRef](#)]

37. Ferraris, G.M.S.; Schulte, C.; Buttiglione, V.; De Lorenzi, V.; Piontini, A.; Galluzzi, M.; Podesta, A.; Madsen, C.D.; Sidenius, N. The interaction between uPAR and vitronectin triggers ligand-independent adhesion signalling by integrins. *EMBO J.* **2014**, *33*, 2458–2472. [[CrossRef](#)]
38. Blasco, M.T.; Navas, C.; Martín-Serrano, G.; Graña-Castro, O.; Lechuga, C.G.; Martín-Díaz, L.; Djurec, M.; Li, J.; Morales-Cacho, L.; Esteban-Burgos, L.; et al. Complete regression of advanced pancreatic ductal adenocarcinomas upon combined inhibition of EGFR and C-RAF. *Cancer Cell* **2019**, *35*, 573–587.e6. [[CrossRef](#)]
39. Gandhari, M.; Arens, N.; Majety, M.; Dorn-Beineke, A.; Hildenbrand, R. Urokinase-type plasminogen activator induces proliferation in breast cancer cells. *Int. J. Oncol.* **2006**, *28*, 1463–1470. [[CrossRef](#)]
40. Henke, E.; Nandigama, R.; Ergün, S. Extracellular Matrix in the Tumor Microenvironment and Its Impact on Cancer Therapy. *Front. Mol. Biosci.* **2019**, *6*, 160. [[CrossRef](#)]
41. Javadi, S.; Zhiani, M.; Mousavi, M.A.; Fathi, M. Crosstalk between Epidermal Growth Factor Receptors (EGFR) and integrins in resistance to EGFR tyrosine kinase inhibitors (TKIs) in solid tumors. *Eur. J. Cell Biol.* **2020**, *99*, 151083. [[CrossRef](#)]
42. Tai, Y.L.; Chu, P.Y.; Lai, I.R.; Wang, M.Y.; Tseng, H.Y.; Guan, J.L.; Liou, J.Y.; Shen, T.L. An EGFR/Src-dependent beta4 integrin/FAK complex contributes to malignancy of breast cancer. *Sci. Rep.* **2015**, *5*, 16408. [[CrossRef](#)] [[PubMed](#)]
43. Zheng, Y.; Lu, Z. Paradoxical roles of FAK in tumor cell migration and metastasis. *Cell Cycle* **2009**, *8*, 3474–3479. [[CrossRef](#)]
44. Mitra, S.K.; Hanson, D.A.; Schlaepfer, D.D. Focal adhesion kinase: In command and control of cell motility. *Nat. Rev. Mol. Cell Biol.* **2005**, *6*, 56–68. [[CrossRef](#)] [[PubMed](#)]
45. Ilić, D.; Furuta, Y.; Kanazawa, S.; Takeda, N.; Sobue, K.; Nakatsuji, N.; Nomura, S.; Fujimoto, J.; Okada, M.; Yamamoto, T.; et al. Reduced cell motility and enhanced focal adhesion contact formation in cells from FAK-deficient mice. *Nature* **1995**, *377*, 539–544. [[CrossRef](#)] [[PubMed](#)]
46. Zheng, Y.; Xia, Y.; Hawke, D.; Halle, M.; Tremblay, M.L.; Gao, X.; Zhou, X.Z.; Aldape, K.; Cobb, M.; Xie, K.; et al. FAK Phosphorylation by ERK Primes Ras-Induced Tyrosine Dephosphorylation of FAK Mediated by PIN1 and PTP-PEST. *Mol. Cell* **2009**, *35*, 11–25. [[CrossRef](#)]
47. Chude, C.I.; Amaravadi, R.K. Targeting Autophagy in Cancer: Update on Clinical Trials and Novel Inhibitors. *Int. J. Mol. Sci.* **2017**, *18*, 1279. [[CrossRef](#)]
48. Rangwala, R.; Chang, Y.C.; Hu, J.; Algazy, K.M.; Evans, T.L.; Fecher, L.A.; Schuchter, L.M.; Torigian, D.A.; Panosian, J.T.; Troxel, A.B.; et al. Combined MTOR and autophagy inhibition: Phase I trial of hydroxychloroquine and temsirolimus in patients with advanced solid tumors and melanoma. *Autophagy* **2014**, *10*, 1391–1402. [[CrossRef](#)]
49. Karasic, T.B.; O'Hara, M.H.; Loaliza-Bonilla, A.; Reiss, K.A.; Teitelbaum, U.R.; Borazanci, E.; De Jesus-Acosta, A.; Redlinger, C.; Burrell, J.A.; Laheru, D.A.; et al. Effect of Gemcitabine and nab-Paclitaxel With or Without Hydroxychloroquine on Patients With Advanced Pancreatic Cancer: A Phase 2 Randomized Clinical Trial. *JAMA Oncol.* **2019**, *5*, 993–998. [[CrossRef](#)]
50. Dhillon, A.S.; Hagan, S.; Rath, O.; Kolch, W. MAP kinase signalling pathways in cancer. *Oncogene* **2007**, *26*, 3279–3290. [[CrossRef](#)]
51. Aliabadi, F.; Sohrabi, B.; Mostafavi, E.; Pazoki-Toroudi, H.; Webster, T.J. Ubiquitin–proteasome system and the role of its inhibitors in cancer therapy. *Open Biol.* **2021**, *11*, 200390. [[CrossRef](#)] [[PubMed](#)]
52. Metrangolo, V.; Ploug, M.; Engelholm, L.H. The Urokinase Receptor (uPAR) as a “Trojan Horse” in Targeted Cancer Therapy: Challenges and Opportunities. *Cancers* **2021**, *13*, 5376. [[CrossRef](#)] [[PubMed](#)]
53. Simon, M.; Jorgensen, J.T.; Juhl, K.; Kjaer, A. The use of a uPAR-targeted probe for photothermal cancer therapy prolongs survival in a xenograft mouse model of glioblastoma. *Oncotarget* **2021**, *12*, 1366–1376. [[CrossRef](#)] [[PubMed](#)]
54. Carlsen, E.A.; Loft, M.; Loft, A.; Berthelsen, A.K.; Langer, S.W.; Knigge, U.; Kjaer, A. Prospective Phase II Trial of Prognostication by ⁶⁸Ga-NOTA-AE105 uPAR PET in Patients with Neuroendocrine Neoplasms: Implications for uPAR-Targeted Therapy. *J. Nucl. Med.* **2022**, *63*, 1371–1377. [[CrossRef](#)]
55. Mahmood, N.; Arakelian, A.; Khan, H.A.; Tanvir, I.; Mazar, A.P.; Rabbani, S.A. uPAR antibody (huATN-658) and Zometa reduce breast cancer growth and skeletal lesions. *Bone Res.* **2020**, *8*, 18. [[CrossRef](#)]

Disclaimer/Publisher’s Note: The statements, opinions and data contained in all publications are solely those of the individual author(s) and contributor(s) and not of MDPI and/or the editor(s). MDPI and/or the editor(s) disclaim responsibility for any injury to people or property resulting from any ideas, methods, instructions or products referred to in the content.